IN-91
61182-CR
25P.

Semi-Annual Status Report

Hydrogen Emission from Jupiter:

Hydrogen Emission from Sunlit Atmosphere of Saturn

NASA Grant NAG-5-560

Submitted to

National Aeronautics and Space Administration

by

D. E. Shemansky and J. B. Holberg

April, 1987

ABSTRACT

Successful IUE observations of the equatorial sunlit atmosphere of Jupiter and Saturn have been obtained. Spectra containing atomic and molecular hydrogen and solar reflection continuum emissions have been analyzed, with the purpose of determining the long term temporal behavior of the electroglow process. Quantitative estimates have been established for the first time using a model analysis of the short wavelength region of the spectrum. Both systems show varying degrees of long term variability in hydrogen emission rate, but the time scale is too short to determine whether there is a dependence on solar cycle activity. As part of the emission modeling program, a preliminary point source spreading function for the IUE SWP instrument has been established, suggesting a wavelength dependence in spectral line width different from previous analyses. Further IUE observations are planned for both Jupiter and Saturn.

INTRODUCTION; OBJECTIVES

JUPITER

A question of recognized importance to the understanding of the source and flow of energy in Jupiter's atmosphere, is the long term behavior of the EUV emissions. The initial epoch for usable observations relevant to this question is ~1970. The principle reference points are rocket observations in 1968-72, Pioneer 10 (P10) and Voyager (V) spacecraft encounters in 1973 and 1979 near the times of solar minimum and maximum activity respectively, and IUE measurements beginning in 1978. Recent reanalysis of rocket observations obtained originally by Giles et al. (1976), together with the P10, Voyager, and IUE data indicate that the H_2 band emissions have remained relatively constant, while the H Lyα emission has varied in intensity by an order of magnitude (Shemansky and Judge 1986; Appendix A). The more recent IUE measurements in this series (1985-1986) which have now provided a measure of both H Lyα and H_2 emissions, with the application of spectral models, suggest that the H_2 bands may have increased in brightness at solar minimum whereas the H

Lyα values decreased. This result contrasts with H Lyα measurements of Uranus over the 1982-1985 period in which there is no long term variation (Clarke et al. 1986). Table 1 shows a summary of results. On this basis Jupiter exhibits a substantially larger variation at the H Lyα emission rate than the solar source between minimum and maximum activity. The H Lyα bulge phenomenon showing longitudinal variation in emission rate is unique to Jupiter. The proposed bulge mechanism (Shemansky 1985) requires particle energy deposition in the exosphere, a symptom of which is the observed equatorial H_2 Rydberg bands. The apparent strong variability of the H Lyα emission both in absolute terms and in relation to the H_2 Rydberg systems, is basically not understood, but it appears to imply a changing abundance of H forced primarily by variations in loss rate rather than production rate.

The April 1985 and November 1986 IUE results obtained in this program show a reduced absolute H Lyα intensity, but not to the extent obtained from the equivalent results near solar minimum in 1974. The analysis of the 1985, 1986 measurements also have obtained a measure of H_2 Rydberg brightness which may have increased relative to 1979. The reason for an apparent decreased abundance of atomic hydrogen in the face of an increase in the major dissociation source is an interesting mystery. Further investigation is required to determine the extent of the dependence on the solar cycle.

It should be emphasized that although the brightness of the strong Jovian H Lyα line has been monitored since shortly after the launch of IUE, little of this data can be used to establish the corresponding intensities of the H_2 band emissions. These emissions are complementary to the H Lyα intensity, providing a spectroscopic diagnostic of the dissociation and energy deposition rates. Understanding the role played by solar EUV radiation in catalyzing this emission will require knowledge of the behavior of the Lyα and H_2 band components throughout the solar cycle.

SATURN

We propose to obtain further observations of Saturn's sunlit atmospheric emissions, on the basis of preliminary analysis of very recent measurements obtained in the 9th year IUE program on 1986

DOY 252 and 254. These results show a mean H Lyα brightness a factor of 5 below the value measured by Voyager 1 in November 1980. The details of the analysis indicate that the IUE and Voyager results can be directly compared as discussed below, and we conclude that the apparent change in emission brightness is real. The present result is remarkable because the disk averaged brightness of Saturn in H Lyα (0.88 $\pm$ 0.2 kR) is less than the mean value obtained for Uranus by Clarke et al. (1986). The Saturn disk averaged brightness in H Lyα radiation has not been monitored on a frequent basis so that the time scale of the variation is not well defined. Since the launch of the IUE observatory and the Voyager encounters with the outer planets it has become apparent that, contrary to our expectations, the solar UV flux contributes only a small fraction of the energy deposited in the upper atmospheres of Saturn and Jupiter (Broadfoot, et al, 1981a, Broadfoot et al., 1981b; Shemansky, 1985; Yelle, et al., 1986. Evidence for this is the high exospheric temperatures (1000 K for Jupiter, 420 K for Saturn and 800 K for Uranus), the intense, non- auroral, H_2 band emissions (3 kR from Jupiter and 1 kR from Saturn) and the H Lyα to H_2 band brightness ratio which indicates a high altitude, collisional source for both emissions. These developments imply that the measured solar UV flux can no longer be used as the sole input for calculations of the physical state of Saturnian and Jovian upper atmospheres. Rather, we must rely on the H_2 band brightness to measure the energy deposition and infer the exospheric temperature, ionization rate and atomic H mixing ratio in the upper atmospheres (Table 2 shows estimates of dissociation rates based on Voyager data). Fortunately our understanding of the properties of the H_2 molecule, and consequently synthetic spectra, have advanced sufficiently to allow the accurate determination of total emission brightness, energy deposition and electron temperature (given a sufficient signal to noise ratio) from the measured H_2 band spectrum (Shemansky et al., 1985; Shemansky, 1985). Similarly, the H Lyα line is produced predominantly by collisional excitation rather than resonant scattering of solar Lyα. The resonant scattered contribution is less than 50% on both Saturn and Jupiter [Shemansky, 1985; Yelle et al., 1986]. For this reason the H Lyα to H_2 band brightness ratio directly reflects the atomic H mixing ratio and hence the altitude of the excitation source. The H Lyα to H_2 band brightness ratio provides an important clue to the nature of the

underlying energy source and the physical state of the upper atmosphere.

The relative instability of Jupiter and Saturn in apparent abundance of atomic hydrogen must carry clues to the source process if the nature of the variability can be identified. It is not clear what the relationship to solar cycle is, because all three outer planets, Jupiter, Saturn, and Uranus according to available data show different behaviors in relation to solar activity.

RESULTS; DISCUSSION

JUPITER

We now have an IUE point of reference in August 1984, April 1985, and November 1986. The analysis of this data (Table 1, Figure 1) shows a moderately reduced H Lyα intensity, but a relative bulge amplitude roughly the same as that observed by Voyager. This appears to imply that the H Lyα is excited at about the same atmospheric and ionospheric density levels as in 1979. The solar reflection continuum is at the same level as that obtained by both Voyager and IUE observations in 1979 with the exception of the 1986 result which shows a value 16% larger (Table 1). H_2 band intensities obtained from model calculations compared to the April 1985 IUE data indicate values that are basically the same as an analysis of the Clarke, Moos and Feldman (1982) results, I_S (H_2 Lyα+W_R) = 4.4$\pm$1.6 kR. This value is ~45% larger than the Voyager measurement in 1979. Analysis of the November 1986 spectrum (Figure 2) gives a value 5.4 $\pm$1.7 kR, moderately higher, than the 1985 and earlier value, but about a factor of~ 2 larger than the Voyager value of I_S (H_2 Lyα+W_R) = 3.0 kR. We have proposed further IUE observations of Jupiter to extend the data base further into the solar minimum period. The additional data we are proposing to obtain here would be composed of a series of bracketed SWP exposures designed to measure H Lyα as well as the fainter H_2 features. These data would characterize the Jovian equatorial emission under solar minimum conditions. The importance of obtaining an equatorial H_2 emission spectrum lies in the fact that the emission is clearly unaffected by hydrocarbon absorption, and provides a direct measure of energy deposition rates.

SATURN

We have obtained measurements of the Saturn electroglow spectrum on 1986 DOY 252 and 254 in this program. Observing conditions were remarkably good. Analysis of the data requires relatively more model analysis than is the case for Jupiter, in order to account for extinction effects, geocorona, and non uniformity of the source in the field of view.

Table 3 shows a comparison of earlier results. The corrections for foreground and background LISM contributions and foreground geocorona require model calculations that have not yet been made for the Clarke et al.(1981) observations. Moreover at the time of these observations, Saturn was not in a favorable position in respect to extinction effects in the intervening LISM. Crudely estimated extinction coefficients are given in Table 3. The measured H Lyα brightness from IUE is substantially lower than the V1 result, which we attribute mostly to extinction, by the interplanetary medium (ISM/IPM) partly to the analysis method, and possibly partly to variability in the source. The 1980 IUE observations are close enough to solar maximum to constitute a solar maximum reference. Observations in 1986 and 1987 will provide measurements near solar minimum, under much more favorable conditions (see Table 3 for extinction estimate in 1986).

It should be emphasized that although the brightness of the H Lyα line on Saturn has been monitored over much of the lifetime of IUE, little of this data can be used to establish the corresponding intensities of the H_2 band emissions. As we have pointed out H_2 emissions are complementary to the intensity of the H Lyα line, providing a spectroscopic diagnostic of the excitation process. Understanding the role played by solar EUV radiation in stimulating this Saturnian EUV emission will require knowledge of the behavior of both components at conditions of solar maximum and minimum. Unfortunately the observations designed to provide H_2 band intensities in this program have not been reduced to this extent for lack of available time (1986 DOY 252, 254) for analysis. We therefore do not have a measure of how accurately the band emissions can be measured.

The observational sequence in the last program (1986 DOY 252, 254) is shown in Table 4. The Table includes the reduction of the H Lyα brightness. We regard this as the best combination of

exposures required to obtain both H_2 band H Lyα and solar reflection continuum. The reflection continuum albedo is low enough that moderate changes in eddy diffusion coefficient may be detectable.

We require models of the LISM as well as the geocorona in order to properly reduce the data. We have developed a model of the geocorona for this purpose, and we have used the recent Ajello, et al. (1987) model of the LISM to take complete account of the extraneous H Lyα signal in the data. The result of the application of the models is shown in Table 4. This is the only IUE observational data from Saturn that has been analyzed in this way, and it will be necessary for comparative purposes to reanalyze the earlier data obtained by Clarke et al. (1981). Table 4 shows the sequence of observations with the measured H Lyα intensity in Col. 4. Interspersed with the Saturn observations are background data obtained 60" north of the planet. The background is composed of geocoronal and LISM components as estimated in Col. 5 and 6 of Table 4. The component of the LISM in the foreground to the planet is estimated to be 0.463 kR as given in Table 3, using the Ajello, et al. (1987) LISM model. The total LISM intensity in the look direction was 0.622 kR. Although the observed emission brightness varied from ~3.1 kR to ~1.8 kR during the sequence, most of the variation appears to be caused by the geocoronal component, and the derived Saturn emission brightness is basically constant during the sequence with an estimated mean value of IHLyα = 0.88$\pm$.2 kR. The geometry for the 1986 DOY 252, 254 observations is ideal in the sense that the planet is essentially directly upstream from the earth relative to the bulk inflow of the LISM, so that extinction of the planetary signal is at a minimum. However, the observing geometry at the time of the Clarke et al. (1981) observations indicates a substantially larger extinction factor (Table 3). If these estimates are correct the evidence indicates that the Saturn emission brightness in H Lyα has varied by a factor of 5. The inference is that the abundance of atomic hydrogen on the planet must have changed significantly.

The analysis of the 1986 DOY 252, 254 data is incomplete, because there has been insufficient time to reduce line by line data to obtain estimates of the H_2 equatorial emission. We therefore do not have a good assessment of the uncertainties in determining H_2 band intensities. In contrast to

the H Lyα analysis described above, auroral and ring reflection components must be removed from the data in order to analyse the H_2 band electroglow emissions.

DEVELOPMENT OF EMISSION MODELS

We use an H_2 emission model that has been employed extensively in the analysis of both Voyager observations of H_2 emission from Jupiter and Saturn (Shemansky and Ajello, 1983; Shemansky 1985) as well as interpretation of electron excited H_2 emissions in the laboratory (Ajello et al., 1984, Shemansky et al. 1985). We have developed and applied an accurate model of the IUE instrument transmission function for use with our calculations of the emission structure of the H_2 Rydberg systems (see accompanying report). It is composed of a convolution of a gaussian (point source) and a trapezoidal function. The FWHM of the trapezoidal function is constant as a function of wavelength. However on the basis of our analysis of a point source H Lyα line, and results reported by Cassatella et al. (1983), we apply a gaussian function with a linear FWHM dependence on wavelength, ranging from 3.44A at 1216A to 6.40 A at 1900 A. This analysis differs from that of Cassatella et al. at short wavelengths (see accompanying report). The instrument transmission function is clearly an important factor in the analysis of discrete structure, and the variation of the gaussian point source function measurably affects results. We use an H_2 emission model that has been employed extensively in the analysis of both Voyager observations of H_2 emission from Jupiter and Saturn (Shemansky and Ajello, 1983; Shemansky 1985) as well as the interpretation of electron excited H_2 emissions in the laboratory (Shemansky et al., 1985). As far as we are aware it is the most comprehensive model of H_2 emission employed so far.

Figure 2 shows the analysis of the November 1986 spectrum. All of the spectral components are modeled, including solar reflection continuum.

REFERENCES

Ajello, J. M., D. E. Shemansky, T. L. Kwok, and Y. L. Yung, Phys. Rev. A., 29, 636, 1984.

Ajello, J. M., A. I. Stewart, G. E. Thomas, A. Graps, Astrophys. J., June 15, 1987 (in press).

Broadfoot, et al., J. Geophys. Res., 212, 206, 1981.

Broadfoot, et al., J. Geophys. Res., 86, 8259, 1981.

Cassatella, A., J. Barbero, P. Benvenuti. IUE ESA Newsletter #18, Dec. 1983.

Clarke, J. T., H. W. Moos, and P. D. Feldman, Ap.J. Letters, 245, L127, 1981a.

Clarke, J. T. H. W. Moos, and P. D. Feldman, Ap. J., 255, 806, 1982.

Clarke, et a., J. Geophys. Res., 91, 8771, 1986.

Giles, J. W., H. W. Moos, and W. R. McKinney, J. Geophys. Res. 81, 7597, 1976.

Shemansky, D. E., and J. M. Ajello, J. Geophys. Res., 88, 459, 1983.

Shemansky, D. E., J. Geophys. Res., 90, 2673, 1985.

Shemansky, D. E.., J. M. Ajello, and D. T. Hall, Ap.J., 296, 765, 1985.

Shemansky, D. E. and D. L. Judge, submitted, 1986.

Yelle, R. V., B. R. Sandel, D. E. Shemansky, and S. Kumar, J. Geophys. Res., 91, 8756, 1985.

TABLE 1

Jupiter sub-solar brightness with no correction for ISM/IPM extinction

Obs.	Date	I(H_2Ly+WR) (kR)	I(HLyα) (kR)	I(H Lyα) / I(H_2Ly+WR)	(1600A) R/A	III CML	Remarks
Rocket [a]	1972/144	2.4	1.	0.4	50.	100	Disk Average
		3.1	1.5	0.5	74.	100	Calculated Sub-solar Point
Rocket [b]	1978/335		13			106	Disk Average
	1978/335		19			106	Sub-Solar Point
IUE [c]	1979/158				74.		Sub-Solar Point
V2 [d]	1979/187	3.0	16	5.3	76.	240-330	Sub-Solar Point
V2 [d]	1979/187	3.0	22.	7.2	65.	60-150	Sub-Solar Point
IUE [e]	1979/120 -150		15			100	Sub-Solar Point
IUE [e]	1980/120 -180		12			100	Sub-Solar Point
IUE [f]	1985/99	4.4± 1.6	8.0	1.8	76± 6	100	Sub-Solar Point
IUE [f]	1985/99	4.4± 1.6	5.8	1.3	76± 6	280	Sub-Solar Point
IUE [f]	1986/304		8.2	1.6		100	Sub-Solar Point
IUE [f]	1986/304	5.2± 1.5	6.0	1.1	85± 6	280	Sub-Solar Point

a) Judge and Shemansky (1985) analysis of Giles et al. (1976) rocket experiment, E-W H bands distribution shows no limb darkening (Shemansky, 1985)
b) Clarke et al. (1980) rocket experiment
c) Present work, estimate from SWP 5448
d) Shemansky (1985) analysis of V2 data
note: $\frac{I(1600A)}{I(1660A)}$ - 0.43; Table 3 should read "Atmospheric Reflection 1660A; Solar"
e) Clarke et al. (1981a) corrected upward by a factor of 1.16 on 1983 correction to IUE aperture size.
f) Present work Holberg and Shemansky (1985).

TABLE 2
Exobase Production Rates and Escape of Atomic

Hydrogen from the Outer Planets[a]

	Jupiter	Saturn	Uranus
(1)	1.6×10^{30}	3×10^{29}	2×10^{28}
(2)	5.1×10^{9}	1.7×10^{9}	5×10^{8}
(3)	19.	6.	2.3
(4)	0	~10	~80
(5)		1.6×10^{9}	8×10^{8}
(6)		3×10^{28}	1.6×10^{28}
(7)		10^{11}	
(8)		2×10^{4}	2×10^{4}
(9)	5-7.3	2.8-5.3	$\geq 2.$
(10)	3.0×10^{9}	1.0×10^{9}	4.0×10^{8}

[a]These estimates exclude auroral activity (see text).
(1) Dissociation production rate (s^{-1});
(2) ($cm^2\ s^{-1}$)
(3) HI escape energy (eV);
(4) Escape yield (%)
(5) Loss rate (kg yr^{-1});
(6) (atoms/s)
(7) Loss lifetime for 200 km am H_2 (yr)
(8) Exosbase ion density (cm^{-3});
(9) Y_{IS} (Eq. 1)
(10) Ionization Rates (ions $cm^{-2}\ s^{-1}$)

TABLE 3

Rough estimate of extinction by the ISM/IPM for observations of H Lyα

	Date	I(H Lyα) (kR) [a]	τ [b]	Ic(H Lyα) (kR) [c]	$\frac{Ic(H\ Ly\alpha)}{I(H\ Ly+WR)}$	λ_{III}
			Jupiter			
Rocket	1972/144	1.5	0.236	1.9	0.61	100
Rocket	1978/355	19.	0.30	26		100
V2	1979/187	22.	0.0	22.	7.2	60-150
IUE	1980/120 /150	15.	0.30	20.		100
IUE	1980/120 /150	12.	0.30	16.		100
IUE	1985/99	8.	0.236	10.	2.3	100
			Saturn			
IUE[d]	1980/19	0.9	.85	2.2		
IUE[d]	1980/125	0.7	.85	1.5		
V1	1980/316	4.9	0.0	4.9	5.3	
V2	1981/236	3.0	0.0	3.0	2.8	

a) Brightness before correction for extinction
b) Calculated optical thickness (see text)
c) Brightness after correction for extinction
d) Clarke et al. (1981b) corrected upward by factor of 1.16 on basis of 1983 correction to IUE aperture size. Saturn is known to have no limb darkening effect in H Lyα and therefore no limb darkening corrections are applied to the measured data.

TABLE 4

1986 DOY 252 and 254 SATURN IUE OBSERVATIONS OF H LYα

SWP	Exposure Duration (Min)	Scattering Background (FN/S)	ILy-α Observed (kR)	ILy-α Geocorona (kR)	ILy-α ISM (kR)	ILy-α[b] Saturn Emission (kR)
29170[a]	30	---	0.917	0.295	0.622	---
29172	80	2.83	2.862	1.651	0.508	0.976
29173	30	2.65	3.137	2.019	0.508	0.849
29174[a]	15	---	2.276	1.593	0.622	---
29175	15	2.25	2.295	1.220	0.508	0.788
29176	25	2.83	1.979	0.920	0.508	0.765
29177	25	2.50	1.747	0.686	0.508	0.768
29189[a]	30	---	2.166	1.604	0.622	---
29190	30	2.39	2.220	1.124	0.508	0.817
29191	30	2.27	1.903	0.803	0.508	0.822
29192	15	2.37	1.819	0.625	0.508	0.953
WEIGHTED MEAN						0.88± 0.2

a - Sky Background Observation (60" N of Saturn)

b - Implied Saturn Emission = $(I_{OBS} - I_{ISM} - I_{GEOCORNA})/.72$

c - $I(Ly\text{-}a)_{ISM} = [I(Ly\alpha)_{ISM\infty}]^{*}.28 + [I(Ly\alpha)_{ISMSAT}]^{*}0.72$

$I(Ly\alpha)_{ISM\infty} = 0.622$ kR

$I(Ly\alpha)_{ISMSAT} = 0.463$ kR

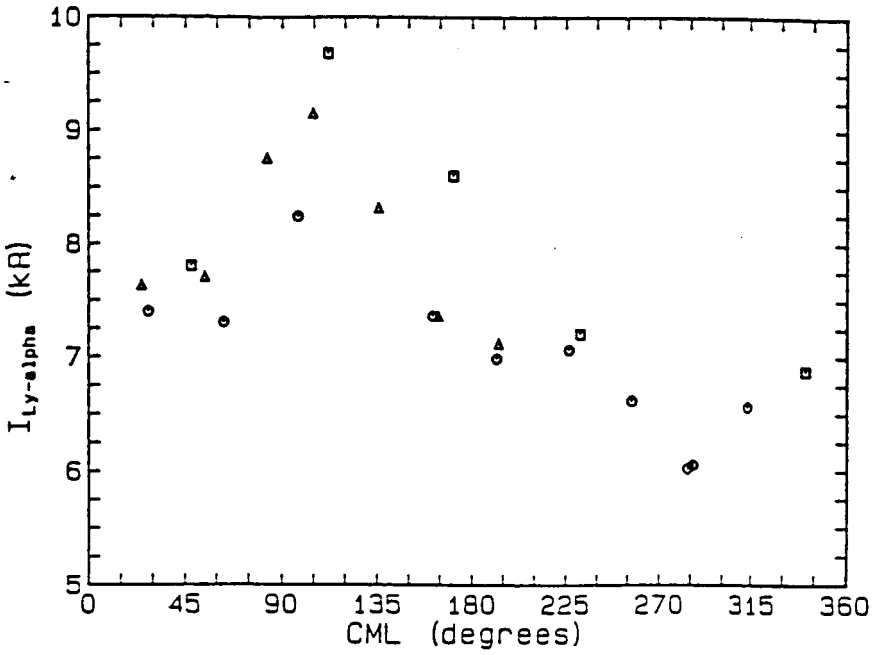

Figure 1

Fig. 1 H Lyα brightness Jupiter center, calculated from IUE measurements in 1984-1986, as a function of CML. Geocoronal and LISM components have been removed using model calculations referenced to interspersed IUE background measurements.

□ August 1984

○ April 1985

△ November 1986

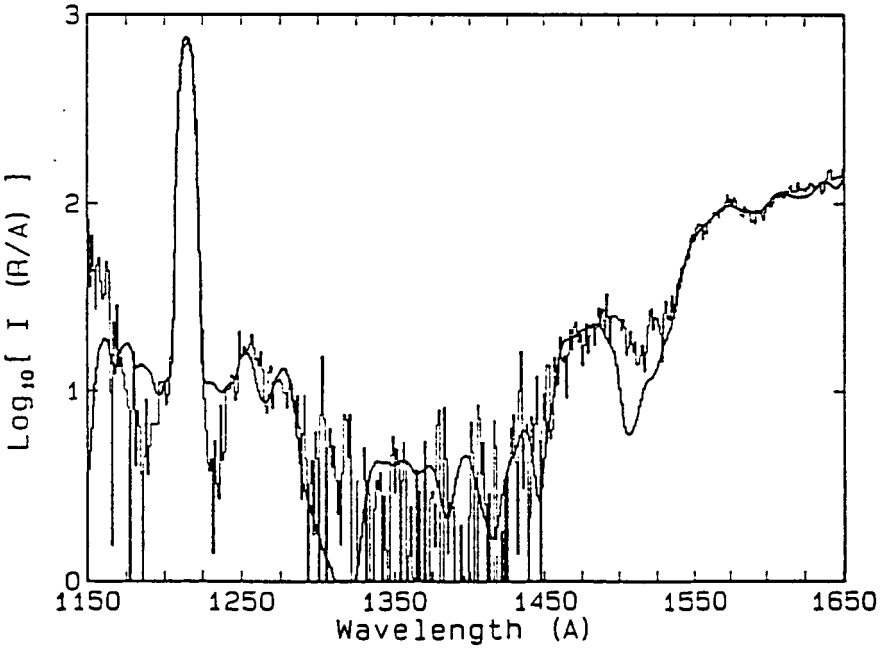

Figure 2

Fig. 2 Reduced composite spectrum of Jupiter obtained November 1986. The data is a combination of SWP29576 (15 min.) SWP29576 (80 min.) and SWP29577 (90 min.) such that the entire spectrum contains unsaturated signal. The heavy overplotted line is a model calculation of electron excited H_2 , combined with an H Lyα line and a model of the solar reflection continuum.

Evidence for Change in Particle Excitation of Jupiter's Atmosphere 1968–1979

D. E. Shemansky

Lunar and Planetary Laboratory

University of Arizona

Tucson, AZ 85721

and

D. L. Judge

Center for Space Sciences

University of Southern California

Los Angeles, CA 90089-1341

January 5, 1987

Submitted to: Journal Geophysical Research

Abstract

Analysis of the Pioneer 10 and rocket observations of disk averaged emission from the sunlit atmosphere of Jupiter indicates that the spectrally integrated EUV brightness was reduced by at least a factor of 2 relative to Voyager spacecraft observations in 1979. Most of the variation is caused by the H Ly α component in the spectrum, which was reduced ~ 1 order of magnitude near the time of solar minimum in 1972-1973. Although the analysis of the data does not produce entirely consistent results, the weight of evidence points to a factor of order ~ 2 lower abundance of HI in Jupiter's atmosphere in 1972-1973 relative to 1979. The low emission rate in H Ly α near the time of solar minimum in this proposed scenario is caused by an electroglow energy deposition rate reduced by a factor of ~ 3. The apparent reduced abundance of HI implies a reduced thermospheric temperature, even under the assumption of a constant electroglow deposition rate.

IUE SWP Point Source and Filled Field Spectral Transmission Function

D. E. Shemansky, J. B. Holberg, and D. T. Hall

Lunar and Planetary Laboratory

University of Arizona, Tucson, AZ 85721

In the analysis of discrete emission spectra obtained with IUE, we have found that it is important to apply an accurate spectral transmission function. In the course of applying model calculations to emission spectra of the outer planets using the SWP camera we have established what we believe to be a more accurate function particularly at the shortest wavelengths. Cassatella et al. (1985) have provided a valuable analysis of the system in both the dispersive and non dispersive coordinates. Figure 6 of the Cassatella et al. (1985) paper shows a plot of the FWHM for the SWP based on point source observations in the large and small aperatures, showing variation in the FWHM width of emission lines as a function of wavelength, using extracted spectra as given by the IUESIPS. Cassatella et al. suggested that resolution was at a peak in the 1300-1400 A region, although uncertainty in the measured widths increased at the shorter wavelengths due to the poor quality of the available sources. Many of the features of major interest in outer planet atmospheric observations occur in the vicinity of the H Lyα line. In order to produce a better measure of the point source spreading function, we obtained a measurement of the H Lyα line in emission from the geocoronal background, using the small aperture. This spectrum in flux numbers is shown in Figure 1. Although the source fills the field of the small aperture, the line is assumed to be equivalent to a point source function, because

the ultimate instrumental resolution is the limiting factor at the solid angle defined by the aperture. A model calculation using a Gaussian function with FWHM = 3.44 Å provides an optimum fit to the line. Figure 1 shows the Gaussian curve integrated over the mean channel interval of the instrument in comparison to the observed line. The fit clearly appears to be exceptionally good. If one applies the data plotted by Cassatella et al. a value FWHM ~ 5.3 Å would be obtained, approximately 50% larger than the present result. On this basis with the trend shown in the Cassatella et al. data we recommend that a linear function be applied to the calculation of the FWHM values of the Gaussian shape as a function of wavelength,

$$\text{FWHM} = a\,\lambda + b, \qquad (\text{Å}) \tag{1}$$

$$1150\ \text{Å} \leq \lambda\ 2000\ \text{Å},$$

where

$$a = 4.444 \times 10^{-3},$$

$$b = -1.984.$$

The quantity FWHM varies from 3.44 Å (@1216Å) to 6.9 Å (@2000Å). Figure 2 shows a plot of the proposed linear FWHM function against the data provided by Cassatella et al., and the present result at 1216 Å. In model calculations for spectra of sources filling the SWP large aperture, we have applied a convolution of the point source function given above with a constant trapezoidal shape function having a full width at the peak of

$$\text{FWP} = 7.24 \qquad (\text{Å}), \tag{2}$$

with a value

$$\text{FWHM} = 9.96 \qquad (\text{Å}) \tag{3}$$

The parameters for the trapezoidal function have been designed to provide a best fit to the H Lyα line of uniform intensity filling the large aperture. Figure 3

shows a direct comparison of 1216 Å and 1800 Å monochromatic lines modeled for a uniform spatially diffuse source, illustrating the effect of the variational point source function. The spectra in this case are given in absolute units, using the IUE photometric calibration curve as it would be applied to real data. Each line is fixed at a brightness of 1R. The Figure 3 plot of differential (R/Å) brightness indicates differences in peak value of the order of 10%, the 1216Å line being significantly narrower. Another effect that should be noted in Figure 3 is that the 1216Å line shows a noticeable asymmetry in its shape. This is caused by the fact that the IUE calibration curve is not flat in the 1150-1300 Å region of the spectrum; the application of the calibration curve to the instrumental transmission function distorts the shape of the resultant calibrated spectrum. At 1216Å this causes very little error in the integrated line intensity (< 1%), but model analysis should follow the procedure described here in order to accurately describe the calibrated spectrum at and below 1216 Å. The FWHM value of the 1216 Å feature in this calculation is 10.5 Å. Note that the calibration curve distorts the shape of the 1216 Å line in Figure 3 sufficiently to cause the peak in the line profile to occur ~ 1 Å shortward of the position of the source line. Attempts to adjust the wavelength scale using calibrated spectra may therefore introduce errors; such adjustments should be made to the flux number spectra prior to application of the calibration curve. From this point of view spectral analysis with or without the use of models should be done using flux number spectra, with a subsequent conversion to absolute quantities; in effect, the calibration process applies conversion factors to photons that do not match the wavelength of the conversion factor, causing distortion of the true instrumental transmission function.

We recommend that model calculations be carried out in a two stage process in which point source gaussian lines are first placed in a buffer with integration channel widths of $\lambda \leq 0.1$ Å. The buffered data is then treated as a monochromatic line source for the trapezoidal transmission function. The resultant convoluted spectrum can then be integrated to match the mean channel width of the IUESIPS data. A code for a normalized trapezoidal function integrated over user selected channel widths is given below.

Reference

Cassatella, A., J. Barbero, D. Benvenuti, On the international ultraviolet explorer (IUE) point spread function at low resolution, IUE Newsletter #24, June 1984, p. 84.

```
0001  FTN4
0002        SUBROUTINE TFUN2(W,WZ,SN1,SN2,WRES,IERR)
0003  C          DES 1/4/83
0004  C        TRAPEZOIDAL TRANSMISSION FUNCTION
0005  C        W= WAVELENGTH OF DELTA FUNCTION LINE
0006  C        WZ=WAVELENGTH OF SHORT WAVELENGTH EDGE OF 1 ST CHANNEL
0007  C              OF THE TRANSFORM DATA FILE
0008  C        SN1=FWHM/WRES , WHERE FWHM IS FWHM OF TRANSMISSION FUNCTION
0009  C        SN2=HWP/WRES  , WHERE HWP IS THE HALF WIDTH OF THE TRAPEZOID PEAK
0010  C        WRES= WIDTH OF DATA CHANNEL IN UNITS OF W
0011  C        IERR=-1 INDICATES OVERRANGE OF TRANS DIMENSION IN COMMON
0012  C       THE DATA DEPOSITED IN THE TRANSFORMED FILE IS I*TRANS
0013  C                 WHERE I IS THE LINE INTENSITY
0014  C        TRANS(25) ON EXIT CONTAINS LINE TRANSMISSION FUNCTION
0015  C                 IN LOCATIONS TRANS(1) THRU TRANS(NMAX)
0016  C        MINCH=FIRST LOCATION IN DATA FILE FOR SUMMATION OF THE
0017  C                 TRANSFORMED LINE; SUM I*TRANS(1) INTO MINCH
0018  C        MAXCH=LAST LOCATION IN DATA FILE FOR SUMMATION OF THE
0019  C                 TRANSFORMED LINE; SUM I*TRANS(NMAX) INTO MAXCH
0020  C       FIRST CHANNEL IN DATA FILE IS NUMBERED +1
0021  C       WAVELENGTHS INCREASE WITH INCREASING CHANNEL NUMBER
0022  C       THE TRANSMISSION FUNCTION IS NORMALIZED TO 1.00
0023  C       SN2=0.0 DEGENERATES THE FUNCTION TO A TRIANGLE
0024        DIMENSION UF(4),RF(4)
0025        COMMON TRANS(25),NMAX,MINCH,MAXCH,NCH
0026        DATA RF/1.0,-1.0,-1.0,1.0/
0027  C
0028  C
0029  C
0030        IERR=0
0031        SNCH=(W-WZ)/WRES
0032        NCH=IFIX(SNCH)
0033        PCH=SN1-SN2+NCH-SNCH
0034        NP=IFIX(PCH)+1
0035        DEL=PCH-NP
0036        NM=IFIX(2.0*(SN1-SN2)-DEL)
0037        NMAX=NM+1
0038        IF(NMAX.GT.25) GO TO 70
0039        MINCH=NCH+1-NP
0040        MAXCH=MINCH+NM
0041        DO 10 I=1,25
0042     10 TRANS(I)=0.0
0043        UF(1)=0.0
0044        UF(2)=SN1-2.0*SN2
0045        UF(3)=SN1
0046        UF(4)=2.0*(SN1-SN2)
0047        TN=SN1*UF(2)
0048        TN=0.5/TN
0049        DO 60 I=1,NMAX
0050        N=I-1
0051        DO 50 K=1,4
0052        ALPH=N+DEL-UF(K)
0053        IF(ALPH .GE. 0.0) SL=2.0*ALPH+1.0
0054        IF(ALPH .LT. 0.0 .AND. ALPH .GT. -1.0) SL=(ALPH+1.0)**2
0055        IF(ALPH .LE. -1.0) SL=0.0
0056     50 TRANS(I)=TRANS(I)+RF(K)*SL
0057     60 TRANS(I)=TN*TRANS(I)
0058     65 CONTINUE
0059        RETURN
0060     70 IERR=-1
0061        GO TO 65
0062        END
```

Figures

Fig. 1 A comparison of the observed and modeled profile of the Ly α line in the SWP small aperture. The observed profile represents the net flux number spectrum from a 335 m exposure (SWP25630) of the geocoronal Lyα background.

Observed data; oooo.

Model calculation;————————.

An optimal fit to the observed data is shown calculated using a Gaussian profile with FWHM = 3.44 A integrated over channel widths corresponding to the IUE data interval.

Fig. 2 Point Source Gaussian FWHM as a function of wavelength, recommended for use in the analysis of IUE SWP data. The formula for the linear function is given in the text.

□ - FWHM determined from Figure 1.

○ - Small aperture data from Cassatella et al.; 2-3 measurements

● - Small aperture data from Cassatella et al.; 4-9 measurements

Fig. 3 Model calculations of IUE SWP monochromatic lines at 1216A and 1800A, from a spatially diffuse source. The data is calibrated (R/A) using the IUE SIPS calibration function. Each line has an integrated brightness of 1 R. The line shapes are calculated using the convolution of Gaussian point source and Trapezoidal aperture function with parameters given by Eqs. (1) - (3). Distortion and shifting of the peak position of the 1216A line is caused by the strong wavelength dependence of the calibration curve in that region of the spectrum.

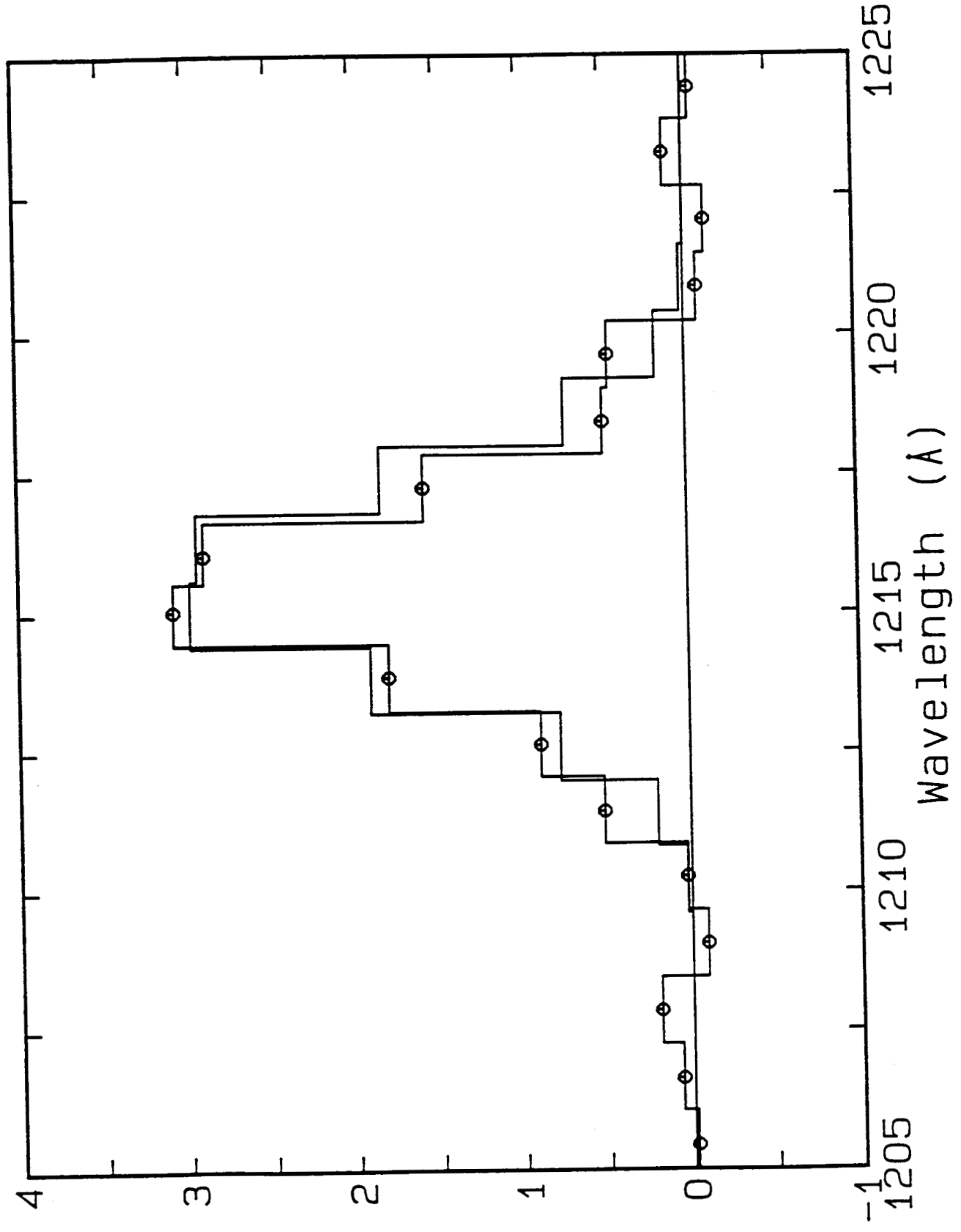
Net Flux (10^4 Flux Numbers)
4
3
2
1
0
-1
1205
1210
1215
1220
1225
Wavelength (Å)

Figure 1

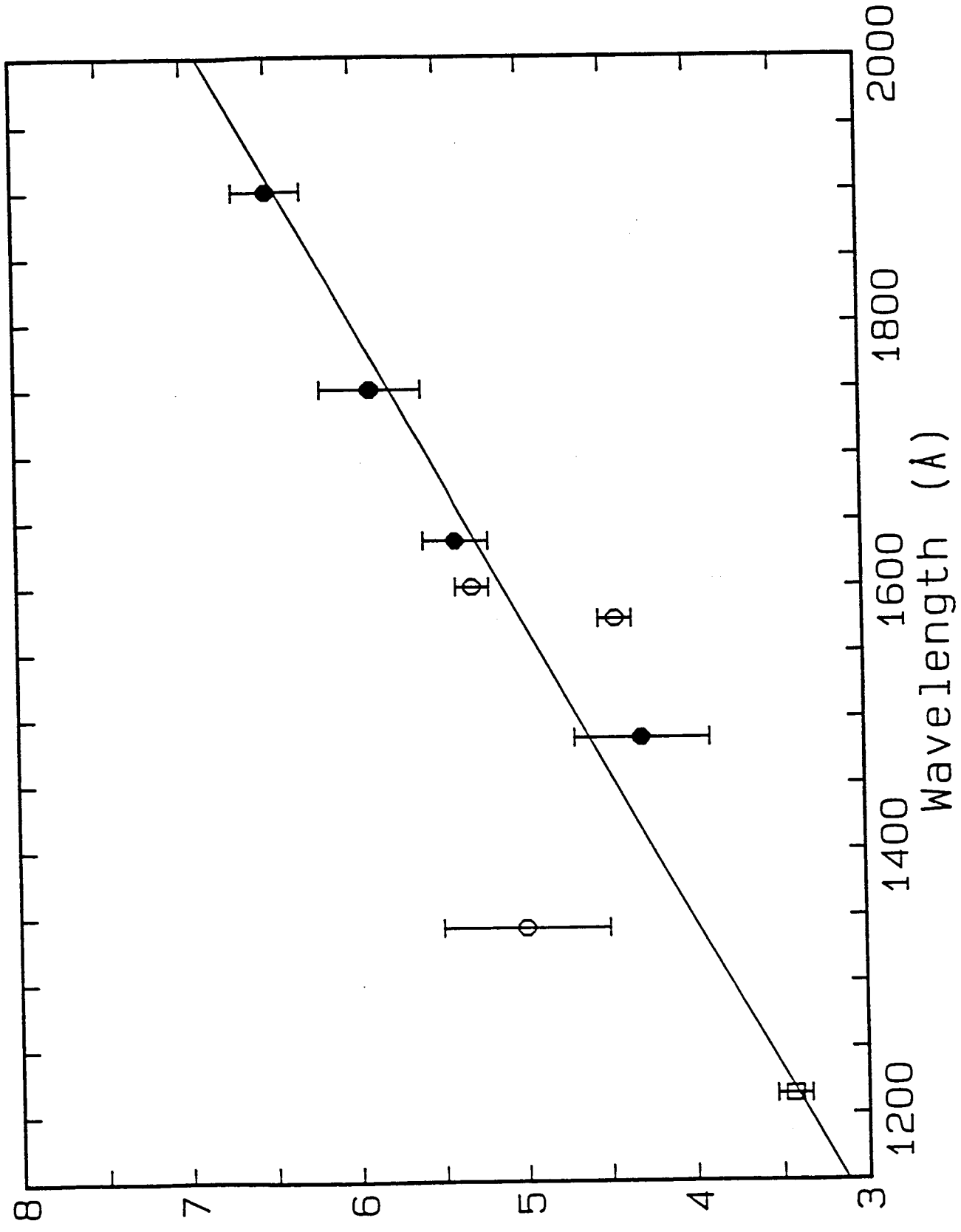
Gaussian FWHM (Å)
8
7
6
5
4
3
1200
1400
1600
1800
2000
Wavelength (Å)

Figure 2

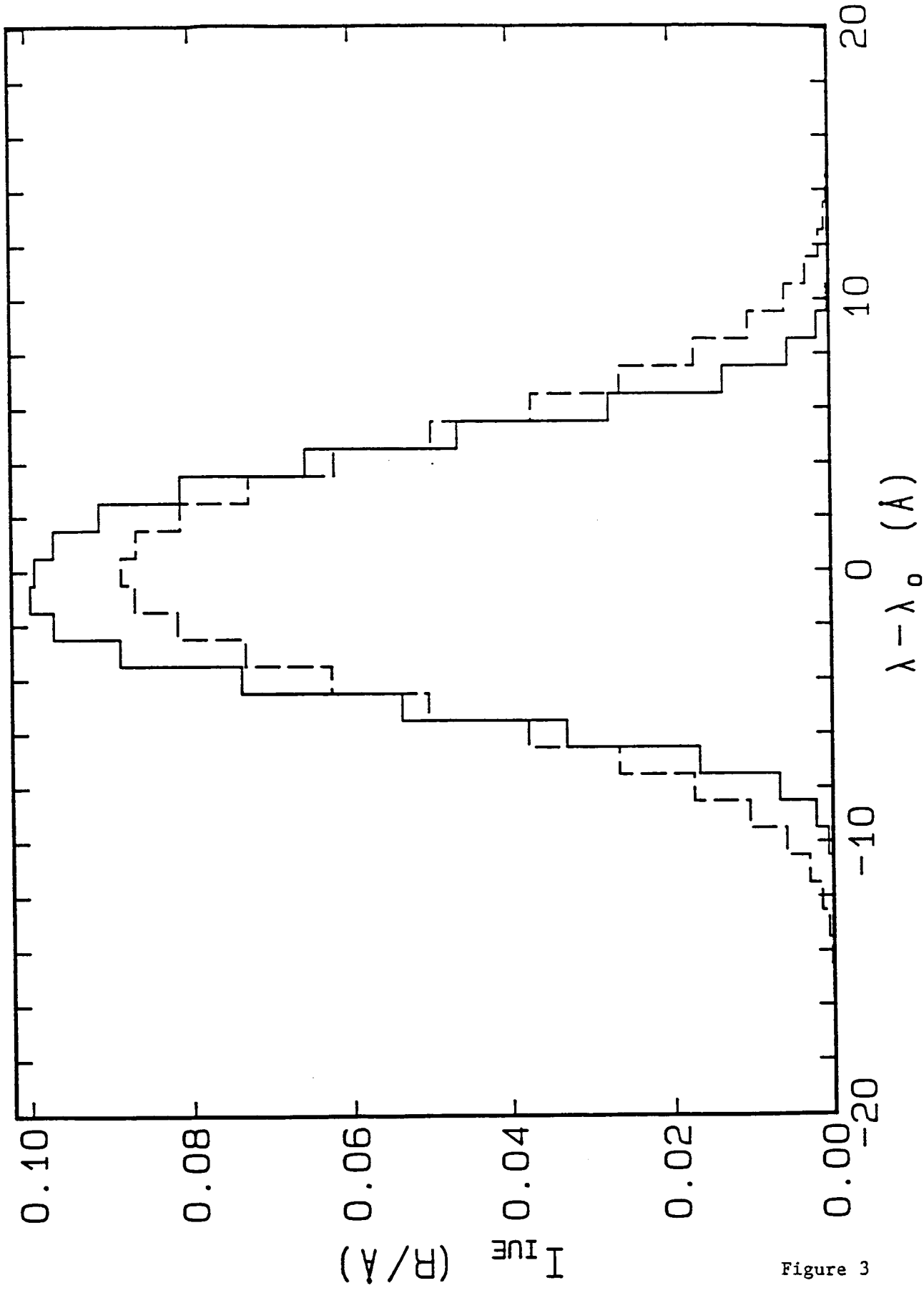

Figure 3